Bonding Properties of a Novel Inorganometallic Complex, $Ru(SnPh_3)_2(CO)_2$(iPr-DAB) (iPr-DAB = *N,N′*-Diisopropyl-1,4-diaza-1,3-butadiene), and its Stable Radical-Anion, Studied by UV−Vis, IR, and EPR Spectroscopy, (Spectro-) Electrochemistry, and Density Functional Calculations

Maxim P. Aarnts,[†] Maikel P. Wilms,[‡] Karin Peelen,[†] Jan Fraanje,[§] Kees Goubitz,[§] František Hartl,*[,†] Derk J. Stufkens,[†] Evert Jan Baerends,[‡] and Antonín Vlček, Jr.*[,∥]

Anorganisch Chemisch Laboratorium, J. H. van 't Hoff Research Institute, Universiteit van Amsterdam, Nieuwe Achtergracht 166, 1018 WV Amsterdam, The Netherlands, Amsterdam Institute for Molecular Studies, Universiteit van Amsterdam, Nieuwe Achtergracht 166, 1018 WV Amsterdam, The Netherlands, Afdeling Theoretische Chemie, Vrije Universiteit, De Boelelaan 1083, 1081 HV Amsterdam, The Netherlands, J. Heyrovský Institute of Physical Chemistry, Academy of Sciences of the Czech Republic, Dolejškova 3, 182 23 Prague, Czech Republic

Received January 12, 1996[⊗]

$Ru(SnPh_3)_2(CO)_2$(iPr-DAB) was synthesized and characterized by UV−vis, IR, ^{1}H NMR, ^{13}C NMR, ^{119}Sn NMR, and mass (FAB^+) spectroscopies and by single-crystal X-ray diffraction, which proved the presence of a nearly linear Sn−Ru−Sn unit. Crystals of $Ru(SnPh_3)_2(CO)_2$(iPr-DAB)·$3.5C_6H_6$ form in the triclinic space group $P\bar{1}$ in a unit cell of dimensions $a = 11.662(6)$ Å, $b = 13.902(3)$ Å, $c = 19.643(2)$ Å, $\alpha = 71.24(2)°$, $\beta = 86.91(4)°$, $\gamma = 77.89(3)°$, and $V = 2946(3)$ Å^3. One-electron reduction of $Ru(SnPh_3)_2(CO)_2$(iPr-DAB) produces the stable radical-anion $[Ru(SnPh_3)_2(CO)_2(iPr\text{-}DAB)]^{\bullet-}$ that was characterized by IR, and UV−vis spectroelectrochemistry. Its EPR spectrum shows a signal at $g = 1.9960$ with well resolved Sn, Ru, and iPr-DAB (H, N) hyperfine couplings. DFT-MO calculations on the model compound $Ru(SnH_3)_2(CO)_2$(H-DAB) reveal that the HOMO is mainly of σ(Sn−Ru−Sn) character mixed strongly with the lowest π^* orbital of the H-DAB ligand. The LUMO (SOMO in the reduced complex) should be viewed as predominantly π^*(H-DAB) with an admixture of the σ(Sn−Ru−Sn) orbital. Accordingly, the lowest-energy absorption band of the neutral species will mainly belong to the σ(Sn−Ru−Sn)→π^*(iPr-DAB) charge transfer transition. The intrinsic strength of the Ru−Sn bond and the delocalized character of the three-center four-electron Sn−Ru−Sn σ-bond account for the inherent stability of the radical anion.

Introduction

Mixed-ligand metal carbonyls (Cr-W, Re, Ru)[1−9] containing α-diimine ligands have been extensively studied because of their interesting photophysical,[2,10,11] photochemical,[1] and redox[4,12,13] properties. Many of these studies focus on the fundamental aspects of the charge-transfer (CT) transitions, which are always directed to the π^* orbital of the α-diimine ligand and can originate either in metal d orbitals (MLCT),[14−16] ligand-localized orbital (LLCT),[7,8,17,18] or a M−L σ-bonding orbital ($\sigma\pi^*$).[19−21] Excitation into low-energy MLCT, LLCT, or $\sigma\pi^*$ transitions is closely related to a ligand-localized reduction of the same complex.[22] This is confirmed by the fact that many photochemically initiated reactions also occur upon reduction of the same complex.[23−25] Well-known in this respect is the photo- or electrocatalyzed reduction of CO_2 to CO by Re(X)-$(CO)_3$(bpy) (X = halide)[4,26−28] or $[Ru(X)_{2-n}(CO)_n(bpy)_2]^{n+}$, $n = 1, 2$.[29,30]

* To whom correspondence should be addressed.
[†] Anorganisch Chemisch Laboratorium, J. H. van 't Hoff Research Institute, Universiteit van Amsterdam.
[‡] Vrije Universiteit.
[§] Amsterdam Institute for Molecular Studies, Universiteit van Amsterdam.
[∥] Academy of Sciences of the Czech Republic.
[⊗] Abstract published in *Advance ACS Abstracts,* August 15, 1996.

(1) Stufkens, D. J. *Coord. Chem. Rev.* **1990**, *104*, 39.
(2) Stufkens, D. J. *Comments Inorg. Chem.* **1992**, *13*, 359.
(3) tom Dieck, H.; Kühl, E. *Z. Naturforsch.* **1982**, *37B*, 324.
(4) Pandey, K. K. *Coord. Chem. Rev.* **1995**, *140*, 37 and references therein.
(5) Vlček, A., Jr.; Víchová, J.; Hartl, F. *Coord. Chem. Rev.* **1994**, *132*, 167.
(6) Lindsay, E.; Vlček, A., Jr.; Langford, C. H. *Inorg. Chem.* **1993**, *32*, 2269.
(7) Nieuwenhuis, H. A.; Stufkens, D. J.; Oskam, A. *Inorg. Chem.* **1994**, *33*, 3212.
(8) Nieuwenhuis, H. A.; Stufkens, D. J.; Vlček Jr., A. *Inorg. Chem.* **1995**, *34*, 3879.
(9) Schanze, K. S.; MacQueen, D. B.; Perkins, T. A.; Cabana, L. A. *Coord. Chem. Rev.* **1993**, *122*, 63.
(10) Kaim, W.; Kohlmann, S. *Inorg. Chem.* **1987**, *26*, 68.
(11) Ernst, S.; Kaim, W. *J. Am. Chem. Soc.* **1986**, *108*, 3578.
(12) Hartl, F.; Luyten, H.; Nieuwenhuis, H. A.; Schoemaker, G. C. *Appl. Spectrosc.* **1994**, *48*, 1522.
(13) Collin, J. P.; Sauvage, J. P. *Coord. Chem. Rev.* **1989**, *93*, 245.
(14) tom Dieck, H.; Stamp, L. *Z. Naturforsch.* **1990**, *45B*, 1369.
(15) van Dijk, H. K.; Kok, J. J.; Stufkens, D. J. *J. Organomet. Chem.* **1989**, *362*, 163.
(16) Balk, R. W.; Stufkens, D. J.; Oskam, A. *Inorg. Chim. Acta.* **1978**, *28*, 133.
(17) Vogler, A.; Kunkely, H. *Comments Inorg. Chem.* **1990**, *9*, 201.
(18) Rossenaar, B. D.; Stufkens, D. J.; Vlček, A., Jr. *Inorg. Chem.* **1996**, *35*, 2902.
(19) Djurovich, P. I.; Watts, R. J. *Inorg. Chem.* **1993**, *32*, 4681.
(20) Kaupp, M.; Stoll, H.; Preuss, H.; Kaim, W.; Stahl, T.; van Koten, G.; Wissing, E.; Smeets, W. J. J.; Spek, A. L. *J. Am. Chem. Soc.* **1991**, *113*, 5606.
(21) Hasenzahl, S.; Hausen, H.; Kaim, W. *Chem.—Eur. J.* **1995**, *1*, 95.
(22) Vlček, A., Jr. *Chemtracts—Inorg. Chem.* **1993**, *5*, 1.
(23) Summers, D. P.; Luong, J. C.; Wrighton, M. S. *J. Am. Chem. Soc.* **1981**, *103*, 5238.
(24) Zoski, C. G.; Sweigart, D. A.; Stone, N. J.; Rieger, P. H.; Mocellin, E.; Mann, T. F.; Mann, D. R.; Gosser, D. K.; Doeff, M. M.; Bond, A. M. *J. Am. Chem. Soc.* **1988**, *110*, 2109.
(25) Hershberger, J. W.; Klingler, R. J.; Kochi, J. K. *J. Am. Chem. Soc.* **1983**, *105*, 61.
(26) Johnson, F. P. A.; George, M. W.; Hartl, F.; Turner, J. J. *Organometallics*, in press.
(27) Kutal, C.; Corbin, J.; Ferraudi, G. *Organometallics* **1987**, *6*, 553.

S0020-1669(96)00042-0 CCC: $12.00

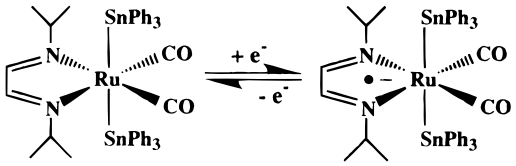

Figure 1. $[Ru(SnPh_3)_2(CO)_2(iPr\text{-}DAB)]^{0,\bullet-}$ complexes studied.

The photochemical and electrochemical properties of such carbonyl−diimine complexes can be fine-tuned by varying the nature of the α-diimine and axial ligands. In the case of the $Re(L)(CO)_3(\alpha\text{-diimine})$[31,32] or $Ru(L)_2(CO)_2(\alpha\text{-diimine})$[33,34] complexes, their properties change profoundly when covalently bonded axial ligands, usually an alkyl, benzyl, or another metal fragment, are introduced. For M−C or M−M′ bonds, the σ-bonding orbital is energetically high-lying and close to the metal dπ and α-diimine π^* orbitals. Hence, the σ-electrons might well become involved in the excitation or redox processes. For Ru complexes, the simultaneous presence of two *trans*-oriented M−L σ-bonds is expected[21] to affect the bonding within the Ru(α-diimine) fragment substantially and lead to new and unusual spectroscopic and redox properties. More knowledge of the special properties of these complexes is important because of their potential use as luminophores, photosensitisers, or redox-catalysts. Herein, we describe the first inorganometallic complex of this type, $Ru(SnPh_3)_2(CO)_2$(iPr-DAB) and its stable radical-anion $[Ru(SnPh_3)_2(CO)_2(iPr\text{-}DAB)]^{\bullet-}$ (Figure 1), which contain a nearly linear Sn−Ru−Sn structural moiety. We have aimed at the understanding of the bonding in these complexes, of effects on the electron-density distribution brought about by the presence of two axial covalent Ru−Sn bonds, and of their spectroscopic and redox consequences.

Experimental Section

Materials. All chemicals were purchased from Janssen Chimica unless stated otherwise. Solvents for spectroscopic experiments were of analytical grade, distilled from sodium wire (THF, hexane) or CaH_2 (CH_3CN). The Silica 60 (Merck) used for the purification of the complexes by column chromatography was activated by heating it overnight *in vacuo* at 180 °C, and it was stored under nitrogen. The supporting electrolyte Bu_4NPF_6 (Aldrich) was dried overnight *in vacuo* at 80 °C. Ferrocene (Fc) (BDH) and $SnClPh_3$ were used without further purification.

Synthesis of $Ru(SnPh_3)_2(CO)_2$(iPr-DAB). First, $Ru(Cl)(SnPh_3)(CO)_2$(iPr-DAB) was synthesized similarly to $Ru(I)(Me)(CO)_2$(iPr-DAB)[7], by reaction of $Ru_3(CO)_{12}$ (Strem), iPr-DAB,[35] and $SnClPh_3$ in hexane. To a solution of 342 mg (0.5 mmol) of $Ru(Cl)(SnPh_3)(CO)_2$(iPr-DAB) in 50 mL of THF, 0.6 mL of sodium−potassium (3:1) alloy was added and the solution was stirred until the color changed from blue green into deep red indicating that the reduction to $[Ru(SnPh_3)(CO)_2(iPr\text{-}DAB)]^-$ was completed.[36] After removal of the excess of NaK by filtration over a G4 frit, the extremely air-sensitive anion was directly added to a small excess of solid $SnClPh_3$ (212 mg, 0.55 mmol) and stirred for a few minutes. Further manipulations of the photolabile product were performed under exclusion of light. After the solvent had been removed by evaporation *in vacuo*, the complex was purified by column chromatography on activated Silica 60, using a hexane/THF mixture in a 9:1 (v:v) ratio as an eluent. The solvents were removed by evaporation *in vacuo*. $Ru(SnPh_3)_2(CO)_2$(iPr-DAB) was obtained in 60% yield as a pink powder.

Characterization data for $Ru(SnPh_3)_2(CO)_2$(iPr-DAB) follow. UV−vis (THF): $\lambda_{max} = 511$ nm ($\epsilon = 6000$ M^{-1} cm^{-1}). IR (THF): ν(CO) = 2005 vs, 1952 vs cm^{-1}. ^{1}H NMR (300.13 MHz, C_6D_6): δ (ppm) = 7.58 (85% d, 15% dd, ^3J(H,H) = 6.3 Hz, $^3J(^{117/119}Sn,H)$ = 76.4 Hz, 12H, Sn(*o*-C_6H_5)), 7.17 (m, 18H, Sn(*m*-/*p*-C_6H_5)), 6.90 (68% s, 30% d, 2% t, $^4J(^{117/119}Sn,H)$ = 26.1 Hz, 2H, imine *H*), 4.35 (sept, ^3J(H,H) = 6.5 Hz, 2H, $(CH_3)_2CH$), 0.71 (d, ^3J(H,H) = 6.5 Hz, 12H, $(CH_3)_2$-CH). ^{13}C NMR (75.46 MHz, C_6D_6): δ (ppm) = 204.6 ($^2J(^{117/119}Sn,^{13}C)$ = 56 Hz, *C*O), 147.3 (imine *C*), 143.4 ($^1J(^{117/119}Sn,^{13}C)$ = 296 Hz, Sn*C*), 137.4 ($^2J(^{117/119}Sn,^{13}C)$ = 33 Hz, SnC*C*), 128.0 ($^3J(^{117/119}Sn,^{13}C)$ = 41 Hz, SnCC*C*), 127.7 ($^4J(^{117/119}Sn,^{13}C)$ = 13 Hz, SnCCC*C*), 64.2 ($C(CH_3)_2$), 24.7 ($C(CH_3)_2$). ^{119}Sn NMR (93.181 MHz, C_6D_6): δ (ppm) = −53. Mass (FAB^+): $(m/z)^+$, (int %) = 997 (3) $[M]^+$, 647 (11) $[M - SnPh_3]^+$, 619 (9) $[M - SnPh_3 - CO]^+$, 591 (3) $[M - SnPh_3 - 2CO]^+$, 570 (9) $[M - SnPh_3 - Ph]^+$, 351 (32) $[SnPh_3]^+$. Anal. Found (calcd) C, 55.60 (55.39); H, 4.60 (4.65); N, 2.74 (2.81).

Crystal Structure Determination. The crystals were grown by slow evaporation of the benzene solvent. A crystal with the approximate dimensions of 0.40 × 0.60 × 0.75 mm was used for data collection on an Enraf-Nonius CAD-4 diffractometer with graphite-monochromated Cu Kα radiation and $\omega-2\vartheta$ scan. A total of 8879 unique reflections was measured within the range $-12 \le h \le 0$, $-15 \le k \le +15$, $-22 \le l \le +20$. Of these, 6455 were above the significance level of $2.5\sigma(I)$. The maximum value of $(\sin\vartheta)/\lambda$ was 0.56 Å^{-1}. Two reference reflections ($\bar{2}0\bar{1}$, $\bar{2}01$) were measured hourly and showed a 6% decrease during the 100 h collection time, which was corrected for. Unit-cell parameters were refined by a least-squares fitting procedure using 23 reflections with $72° < 2\vartheta < 93°$. Corrections for Lorentz and polarization effects were applied. The structure was solved by the PATTY/ORIENT/PHASEX option of the DIRDIF91 program system.[37,38] The hydrogen atoms were placed in calculated positions. After isotropic refinement of the starting model, a ΔF synthesis revealed a number of peaks (21) which could be interpreted as three complete benzene molecules and one-half of a benzene molecule (completed by the center of symmetry). Benzene was the solvent used during the crystallization of the compound. Full-matrix least-squares refinement on F was carried out, anisotropic for Ru and Sn and isotropic for the remainder of the atoms, keeping the hydrogen atoms fixed at their calculated position with $U = 0.05$ Å^2, and it converged to $R = 0.121$, $R_w = 0.180$, and $(\Delta/\sigma)_{max} = 0.10$. The fact that only the heavy atoms could be refined anisotropically and the rather high R factor and residual electron density are probably due to a low crystal quality, which is also reflected in the fact that there are 3.5 solvent molecules present in the asymmetric unit. A weighing scheme $w = (5.3 + F_{obs} + 0.014F_{obs}^2)^{-1}$ was used. An empirical absorption correction (DIFABS)[39] was applied, with coefficients in the range 0.37−2.79. The secondary isotropic extinction coefficients[40,41] were refined to Ext = 0.07(3). A final difference Fourier map revealed a residual electron density between −4.2 and 4.0 e Å^{-3} in the vicinity of the heavy atoms. Scattering factors were taken from Cromer.[42,43] The anomalous scattering of the Ru and Sn atoms was taken into account.[44]

(28) Christensen, P.; Hamnett, A.; Muir, A. V. G.; Timney, J. A. *J. Chem. Soc., Dalton Trans.* **1992**, 1455.
(29) Ishida, H.; Terada, T.; Tanaka, K.; Tanaka, T. *Inorg. Chem.* **1990**, *29*, 905.
(30) Tanaka, H.; Nagao, H.; Peng, S. M.; Tanaka, K. *Organometallics* **1992**, *11*, 1450.
(31) Rossenaar, B. D.; Kleverlaan, C. J.; van de Ven, M. C. E.; Stufkens, D. J.; Oskam, A.; Goubitz, K.; Fraanje, J. *J. Organomet. Chem.* **1995**, *493*, 153.
(32) Rossenaar, B. D.; Kleverlaan, C. J.; Stufkens, D. J.; Oskam, A. *J. Chem. Soc., Chem. Commun.* **1994**, 63.
(33) Nieuwenhuis, H. A.; van de Ven, M. C. E.; Stufkens, D. J.; Oskam, A.; Goubitz, K. *Organometallics* **1995**, *14*, 780.
(34) Nieuwenhuis, H. A.; van Loon, A.; Moraal, M. A.; Stufkens, D. J.; Oskam, A.; Goubitz, K. *J. Organomet. Chem.* **1995**, *492*, 165.
(35) Bock, H.; tom Dieck, H. *Chem. Ber.* **1967**, *100*, 228.
(36) Aarnts, M. P.; Peelen, K.; Hartl, F.; Stufkens, D. J. To be submitted for publication.
(37) Smits, J. M. M.; Behm, H.; Bosman, W. P.; Beurskens, P. T. *J. Crystallogr. Spectrosc. Res.* **1991**, *18*, 447.
(38) Motherwell, W. D. S.; Clegg, W. PLUTO. Program for Plotting Molecular and Crystal Structures. University of Cambridge, U.K., 1978.
(39) Walker, N.; Stuart, D. *Acta Crystallogr.* **1983**, *A39*, 158.
(40) Zachariasen, W. H. *Acta Crystallogr.* **1967**, *A23*, 558.
(41) Larson, A. C. In *Crystallographic Computing*; Ahmed, F. R., Hall, S. R., Huber, C. P., Eds.; Munksgaard: Copenhagen, 1969; pp 291−294.
(42) Cromer, D. T.; Mann, J. B. *Acta Crystallogr.* **1968**, *A24*, 321.
(43) Cromer, D. T.; Mann, J. B. *International Tables for X-Ray Crystallography*; Kynoch Press: Birmingham, 1974; Vol. IV, p 55.
(44) Cromer, D. T.; Liberman, D. *J. Chem. Phys.* **1970**, *53*, 1891.

Table 1. Crystallographic Data for $Ru(SnPh_3)_2(CO)_2(iPr\text{-}DAB)$

formula	$C_{46}H_{46}N_2O_2RuSn_2 \cdot 3.5C_6H_6$	V (Å^3)	2946(3)
M_r	997.8	Z	2
cryst syst	triclinic	D_x (gcm^{-3})	1.62
space group	$P\bar{1}$	λ(Cu Kα) (Å)	1.5418
a (Å)	11.662(6)	μ(Cu Kα) (cm^{-1})	141.0
b (Å)	13.902(3)	F(000)	1286
c (Å)	19.643(2)	T (K)	193
α (deg)	71.24(2)	no. of obsd reflcns	6455
β (deg)	86.91(4)		
γ (deg)	77.89(3)	R^a	0.121
		$R_w{}^b$	0.18

[a] $R = \sum_h||F^h_{obs}| - k|F^h_{calc}||/\sum_h|F^h_{obs}|$. [b] $R_w = \sum_h w_h \Delta F^2_h/\sum_h w_h|F^h_{obs}|^2$.

All calculations were performed with XTAL,[45] unless stated otherwise. Attempts to refine all non-hydrogen atoms anisotropically led to nonpositive definite temperature factors. A summary of the crystallographic data is given in Table 1.

Spectroscopic and (Spectro-) Electrochemical Measurements. All sample manipulations were performed under nitrogen atmosphere using Schlenk techniques. Elemental analyses were performed by the Microanalytisches Laboratorium of Dornis und Kolbe, Mülheim a. d. Ruhr, Germany. Fast atom bombardment (FAB) mass spectrometry was carried out using a JEOL JMS SX/SX102A four-sector mass spectrometer, coupled to a JEOL MS-MP7000 data system. The samples were loaded in a matrix solution (nitrobenzyl alcohol) onto a stainless steel probe and bombarded with xenon atoms with an energy of 3 KeV. Electronic absorption spectra were recorded on a Perkin-Elmer Lambda 5 UV−vis spectrophotometer provided with a Model 3600 data station. IR spectra were measured on a BioRad FTS-7 spectrometer. X-band EPR spectra were recorded at room temperature on a Bruker ECS 106 spectrometer with a field modulation of 100 KHz. The frequency was measured with a HP5350B microwave frequency counter. The magnetic field was calibrated with an AEG magnetic field meter. The microwave power incident to the cavity was measured with a HP432B powermeter. The EPR measurement was carried out in a gastight EPR tube attached to a reaction vessel, of ca. 10 mL. In this vessel, a ca. 10^{-3} M solution of the parent complex in THF was chemically reduced by 1% sodium amalgam. After the completion of the reduction (as judged by the color change from red to green), the sample was carefully decanted into the attached EPR tube. The program "ESR-simulations"[46] was used to simulate the spectrum.

Electrochemical measurements were performed with a PA4 (EKOM) potentiostat. Cyclic voltammetry was carried out at a Pt-disk electrode of 0.56 mm^2 apparent surface area. An Ag wire and a Pt gauze were used as pseudoreference and auxiliary electrodes, respectively. The Fc/Fc^+ redox couple served as an internal standard for determination of the reduction potential and the electrochemical reversibility of the reduction step.[47] Concentrations of 10^{-1} M supporting electrolyte (Bu_4NPF_6) and 10^{-3} M $Ru(SnPh_3)_2(CO)_2$(iPr-DAB) in THF were used. IR and UV−vis spectroelectrochemical data were obtained with an OTTLE (optically transparent thin-layer electrochemical) cell equipped with a Pt-minigrid working electrode (32 wires per cm).[48] NaCl windows were used for IR (OTTLE) experiments. For UV−vis (OTTLE) measurements, CaF_2 or quartz windows were employed. The working electrode was carefully masked to avoid spectral interference from the nonelectrolyzed solution.

Computational Details. All calculations were performed using the Amsterdam density functional program package ADF.[49,50] The computational scheme is characterized by the use of a density fitting procedure to obtain accurate Coulomb and exchange potentials in each SCF-cycle, by the accurate and efficient numerical integration[51,52] of the Hamiltonian matrix elements and the possibility to freeze core orbitals. The LSD exchange correlation potential was used,[53] with the Vosko-Wilk-Nusair[54] parametrization of the electron gas data for the local density approximation of the correlation energy. Becke's nonlocal corrections[55,56] to the exchange energy and Perdew's nonlocal corrections[57,58] to the correlation energy were used. A double-ζ STO basis set for H, C, N, and O was used, and a triple-ζ STO basis set for Ru and Sn was employed. The calculations will be referred to, in the remainder of this paper, as "MO calculations" since the Kohn−Sham formulation of density functional theory leads to molecular orbitals with a good physical basis that can be used very well in MO theoretical considerations.[59] All bases were augmented with one polarization function. Transition dipole moments were calculated using the program Dipole.[60] EPR parameters for the radical anion were calculated using the program GATENQ[61] and included Fermi contact terms and dipolar interactions.

Results

Synthesis and Characterization. The $Ru(SnPh_3)_2(CO)_2$(iPr-DAB) complex was prepared according to the reactions in (1), following a procedure discribed elsewhere.[36]

$$\begin{aligned} Ru(Cl)(SnPh_3)(CO)_2(iPr\text{-}DAB) &\xrightarrow{NaK} \\ &Na(K)[Ru(SnPh_3)(CO)_2(iPr\text{-}DAB)] + Na(K)Cl \\ Na(K)[Ru(SnPh_3)(CO)_2(iPr\text{-}DAB)] &\xrightarrow{SnClPh_3} \\ &Ru(SnPh_3)_2(CO)_2(iPr\text{-}DAB) + Na(K)Cl \end{aligned} \quad (1)$$

The pink product is soluble in most common aprotic solvents (hexane, THF, CH_3CN, *etc.*). It is slightly photosensitive in solution but hardly photosensitive in the solid state. It is air stable both in solution and in the solid state. Its characterization by ^1H, ^{13}C, and ^{119}Sn NMR, IR, UV−vis, and FAB^+ mass spectroscopies pointed to the *trans,cis*-$Ru(SnPh_3)_2(CO)_2$(iPr-DAB) formulation. Corresponding data are summarized in the Experimental Section.

Beside the expected features, the ^1H NMR spectrum shows two interesting effects. First, the signals due to the methyl groups of the isopropyl substituents are shifted approximately 0.5 ppm to higher field with respect to the same signals in Ru(Cl)(Me)$(CO)_2$(iPr-DAB)[7] since they are in the vicinity of the shielding cones of the phenyl groups of the $SnPh_3$ ligands which are umbrella-like placed above and under the iPr-DAB ligand. Second, the imine proton signals are shifted ca. 0.4 ppm upfield in $Ru(SnPh_3)_2(CO)_2$(iPr-DAB) compared with those found[62] for Ru(Cl)$(SnPh_3)(CO)_2$(iPr-DAB) in $CDCl_3$. Moreover, the $^4J(^{117,119}Sn,H)$ coupling strongly depends on the axial ligands (*e.g.* 7.0

(45) Hall, S. R.; Stewart, J. M. *XTAL3.0 User's Manual*; Universities of Western Australia and Maryland: Perth, Australia, and College Park, MD, 1990.
(46) Bruns, W.; Schulz, A. *ESR-Simulation*; Universität Stuttgart: Stuttgart, Germany, 1991.
(47) Gagné, R. R.; Koval, C. A.; Lisensky, G. C. *Inorg. Chem.* **1980**, *19*, 2854.
(48) Krejčík, M.; Daněk, M.; Hartl, F. *J. Electroanal. Chem.* **1991**, *317*, 179.
(49) Baerends, E. J.; Ellis, D. E.; Ros, P. *Chem. Phys.* **1973**, *2*, 52.
(50) Baerends, E. J.; Ros, P. *Int. J. Quantum Chem.* **1978**, *S12*, 169.
(51) Boerrigter, P. M.; te Velde, G.; Baerends, E. J. *Int. J. Quantum Chem.* **1988**, *33*, 87.
(52) te Velde, G.; Baerends, E. J. *J. Comput. Phys.* **1992**, *99*, 84.
(53) Parr, R. G.; Yang, W. *Density Functional Theory of Atoms and Molecules*; Oxford University Press: New York, 1989.
(54) Vosko, S. H.; Wilk, L.; Nusair, M. J. *Can. J. Phys.* **1980**, *58*, 1200.
(55) Becke, A. D. *J. Chem. Phys.* **1986**, *84*, 4524.
(56) Becke, A. D. *Phys. Rev.* **1988**, *A38*, 3098.
(57) Perdew, J. P. *Phys. Rev.* **1986**, *B33*, 8822.
(58) Perdew, J. P. *Phys. Rev.* **1986**, *B34*, 7406.
(59) Baerends, E. J.; Gritsenko, O. V.; van Leeuwen, R. In *Chemical Applications of Density-Functional Theory*; Laird, B., Ross, R., Ziegler, T., Eds.; ACS Symposium Series 629; American Chemical Society: Washington, DC, 1996; p 20.
(60) Wilms, M. P. *Internal Report*; Free University Amsterdam: Amsterdam 1995.
(61) Belanzoni, P.; Baerends, E. J.; Van Asselt, S.; Langewen, P. B. *J. Phys. Chem.* **1995**, *99*, 13094.
(62) Aarnts, M. P.; Stufkens, D. J.; Oskam, A.; Fraanje, J.; Goubitz, K. *Inorg. Chim. Acta*, in press.

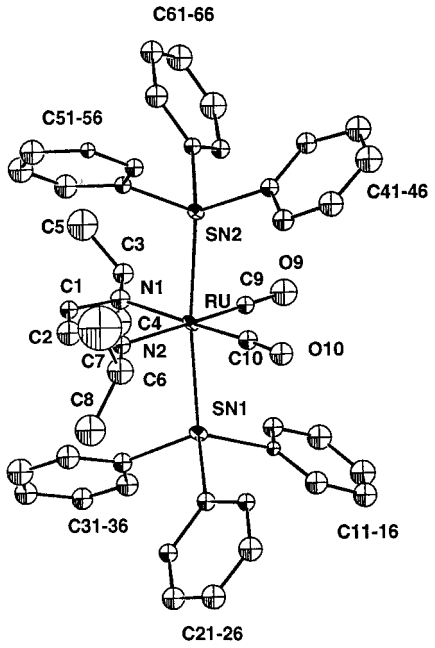

Figure 2. ORTEP drawing of the X-ray structure of $Ru(SnPh_3)_2(CO)_2$(iPr-DAB).

Hz for $Ru(Cl)(SnPh_3)(CO)_2$(iPr-DAB) and 26.0 Hz for $Ru(SnPh_3)_2(CO)_2$(iPr-DAB)). The δ value of −53 ppm for the ^{119}Sn NMR signal of $Ru(SnPh_3)_2(CO)_2$(iPr-DAB) lies in the range +20 to −100 ppm, which is typical for this type of tetrahedrally surrounded Sn atom (M−$SnPh_3$).[63,64]

In the CO-stretching region of the IR spectrum, $Ru(SnPh_3)_2(CO)_2$(iPr-DAB) exhibits two bands of approximately equal intensity at 2004 and 1951 cm^{-1}, respectively (see Figure 3), which is characteristically for *cis*-dicarbonyls.[65] They have been assigned to ν_s(CO) and ν_{as}(CO), respectively.[7] Their wavenumbers are rather small compared with those of related complexes (*e.g.* Ru(I)(Me)$(CO)_2$(iPr-DAB): $\tilde{\nu}$(CO) 2022, 1959 cm^{-1} in THF),[7] due to coordination of the two strongly σ-donating and weakly π-accepting[66] $SnPh_3$ ligands. This leads to an increased π-back-donation to the CO ligands.

Crystal Structure. An ORTEP drawing of the crystal structure of $Ru(SnPh_3)_2(CO)_2$(iPr-DAB) is presented in Figure 2. Selected bond distances and bond angles are collected in Table 2. The complex has a slightly distorted octahedral geometry in which the $SnPh_3$ ligands occupy axial positions. The Ru−Sn bond lengths of 2.686(2) and 2.691(2) Å lie in the range which is typical for Ru−Sn bonds (2.55−2.69Å).[67] The two $SnPh_3$ ligands, which form a nearly linear (173.45(7)°) Sn−Ru−Sn configuration, are in a staggered conformation with respect to their phenyl groups. Interestingly, the central C(1)−C(2) bond (1.39(3) Å) of the iPr-DAB ligand appears to be shorter than the same bond in closely related $Ru(Cl)(SnPh_3)(CO)_2$(iPr-DAB) (1.435(6) Å).[62] At the same time, the C(1)−N(1) and C(2)−N(2) bond distances (1.34(2) and 1.34(3) Å) are elongated with respect to those of the latter complex (1.279(6) and 1.303(6) Å).

Cyclic Voltammetry. The cyclic voltammogram of $Ru(SnPh_3)_2(CO)_2$(iPr-DAB) was recorded in THF at room temperature. The complex is reversibly reduced in an one-electron step at $E_{1/2} = -1.86$ V *vs* Fc/Fc^+. The chemical reversibility is documented by the peak current ratio $I_{p,a}/I_{p,c} = 1$. The electrochemical reversibility is revealed by identical values of ΔE_p (85 mV) for both the complex and the Fc/Fc^+ redox couple (at comparable concentrations), which was used as an internal standard.[47] The reduction step is diffusion-controlled, as $I_{p,c}$ depends linearly on the square root of the scan rate in the range 20 mV/s $\leq \nu \leq$ 500 mV/s. Comparison of the cathodic peak current of $Ru(SnPh_3)_2(CO)_2$(iPr-DAB) with the anodic peak current of ferrocene oxidation points to a transfer of a single electron in the reduction step.

Electrochemical reversibility indicates that the reduction of $Ru(SnPh_3)_2(CO)_2$(iPr-DAB) is not accompanied by any major structural change, apparently producing the $[Ru(SnPh_3)_2(CO)_2(iPr\text{-}DAB)]^{\bullet-}$ radical anion. Chemical reversibility points to its inherent stability, which made it possible to generate and study this species spectroscopically.

Formation and Spectroscopic Properties of $[Ru(SnPh_3)_2(CO)_2(iPr\text{-}DAB)]^{\bullet-}$. Spectroelectrochemistry. Upon the one-electron reduction, the two ν(CO) bands of the parent compound (2004, 1951 cm^{-1}) shift isosbestically to 1975, 1910 cm^{-1} (Figure 3), with a nearly 100% recovery of the original band intensities upon reoxidation. The UV−vis spectra monitored

Table 2. Selected Bond Distances (Å) and Angles (deg) for $Ru(SnPh_3)_2(CO)_2$(iPr-DAB)[a]

Bond Distances			
Ru−Sn(1)	2.686(2)	C(1)−N(1)	1.34(2)
Ru−Sn(2)	2.691(2)	C(2)−N(2)	1.34(3)
Ru−C(9)	1.80(2)	C(3)−N(1)	1.47(3)
Ru−C(10)	1.87(2)	C(6)−N(2)	1.55(3)
Ru−N(1)	2.08(2)	C(9)−O(9)	1.25(2)
Ru−N(2)	2.01(2)	C(10)−O(10)	1.16(3)
C(1)−C(2)	1.39(3)		
Bond Angles			
Sn(1)−Ru−C(9)	86.7(6)	Sn(2)−Ru−N(2)	96.0(4)
Sn(1)−Ru−C(10)	89.3(5)	C(9)−Ru−C(10)	89.6(9)
Sn(1)−Ru−N(1)	96.0(4)	N(1)−Ru−N(2)	77.8(7)
Sn(1)−Ru−N(2)	90.0(4)	C(9)−Ru−N(1)	96.8(8)
Sn(2)−Ru−C(9)	87.6(5)	C(10)−Ru−N(2)	96.0(8)
Sn(2)−Ru−C(10)	87.4(5)	Sn(1)−Ru−Sn(2)	173.45(7)
Sn(2)−Ru−N(1)	87.9(4)		

[a] Standard deviations in parentheses.

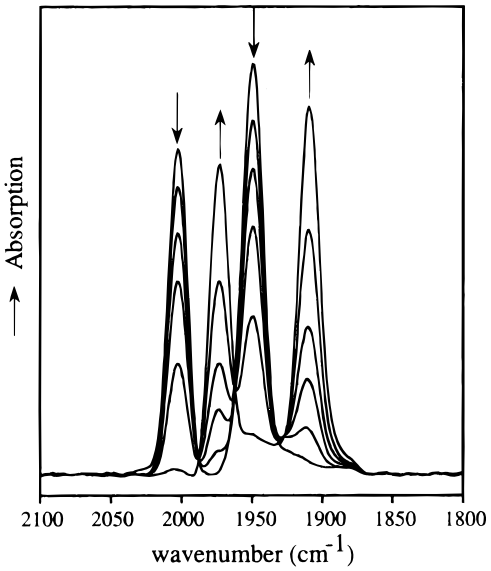

Figure 3. IR spectral changes in the carbonyl stretching region monitored during the electrochemical reduction of $Ru(SnPh_3)_2(CO)_2$(iPr-DAB) in THF at room temperature, using the OTTLE cell.[48]

(63) Harris, R. K.; Kennedy, J. D.; McFarlane, W. In *NMR and the Periodic Table*.; Harris, R. K., Mann, B. E., Eds.; Academic Press: London, 1978; p 342.
(64) Andréa, R. R.; de Lange, W. G. J.; Stufkens, D. J.; Oskam, A. *Inorg. Chim. Acta* **1988**, *149*, 77.
(65) Braterman, P. S. *Metal Carbonyl Spectra*; Academic Press: London, 1975.
(66) Ugo, R.; Cenini, S.; Banati, F. *Inorg. Chim. Acta* **1967**, 451.
(67) Holt, M. S.; Wilson, W. L.; Nelson, J. H. *Chem. Rev.* **1989**, *89*, 11.

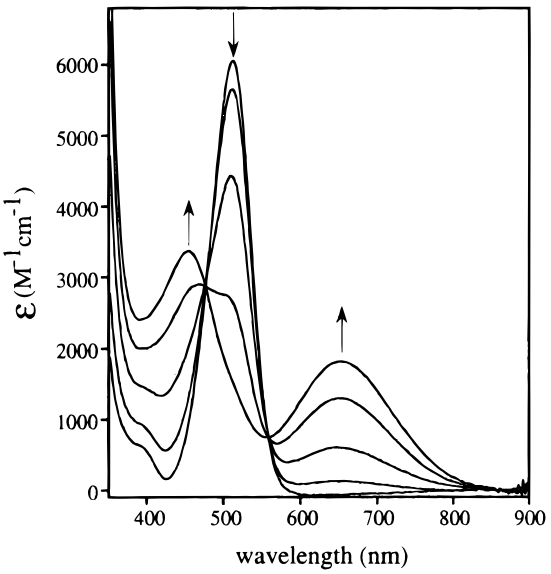

Figure 4. UV−vis spectral changes monitored during the spectroelectrochemical reduction of $Ru(SnPh_3)_2(CO)_2$(iPr-DAB) in THF at room temperature, using the OTTLE cell.[48]

during the spectroelectrochemical reduction (Figure 4) also show a clean, isosbestic conversion. The relative intensities of the IR bands of the reduction product and their wavenumber difference of $\Delta\tilde{\nu} = 65$ cm^{-1} are very similar to those of the parent complex, $\Delta\tilde{\nu} = 53$ cm^{-1}. This implies that the structure of the complex has hardly changed upon reduction.

Thus, the spectroelectrochemical results clearly show that $Ru(SnPh_3)_2(CO)_2$(iPr-DAB) is reduced to an intrinsically stable *trans,cis*-$[Ru(SnPh_3)_2(CO)_2$(iPr-DAB)$]^{\bullet-}$ radical anion which retains the structure of the parent complex. An identical product is formed by reduction with 1% sodium amalgam in THF, as was checked by IR and UV−vis spectroscopies. In fact, $Ru(SnPh_3)_2(CO)_2$(iPr-DAB) is the first complex of the [Ru(L)(L′)$(CO)_2$(α-diimine)]$^{0,+}$ family[12,68] that may be reduced to its radical anion without losing one of the axial ligands.

EPR. In order to understand the bonding properties and the unpaired electron localization in the $[Ru(SnPh_3)_2(CO)_2$(iPr-DAB)$]^{\bullet-}$ radical-anionic complex, its EPR spectrum was studied in detail. The EPR signal, obtained in THF solution, is centered at $g = 1.9960$. It conists of singlet, doublet, and triplet features due to the hyperfine coupling with 0, 1, and 2 $^{117/119}$Sn nuclei, respectively, each of them being further split by the hyperfine coupling with one $^{99/101}$Ru nucleus, two equivalent ^{14}N nuclei, and two pairs of equivalent ^{1}H nuclei, the latter corresponding to the pairs of imine and iPr hydrogens, respectively, (Figure 5, Table 3). The intensity ratios between the singlet, doublet, and triplet components arising from the $^{117/119}$Sn couplings correspond reasonably well to the calculated values: experimental, 100.00:18.26:0.87; calculated, 100.00:17.38:0.77. The tin satellite lines in the spectra are found to be asymmetrically placed about the central line. This is because the hyperfine splitting is sufficiently large to invalidate the high-field approximation in the Breit−Rabit formula.[69] This second-order effect results in a field- (*H*-) dependent $^{117/119}$Sn splitting constant. In order to obtain the experimental a_{Sn} value, corrections to the measured coupling constants were calculated (one iteration cycle) using the correction factors taken from ref 69. To obtain the experimental a_N, a_H, and a_{Ru} values, the central multiplet was computer-simulated. The lines of the simulated multiplet are slightly sharper than the experimental ones since the very small 12 a_H couplings of the four methyl groups of the iPr moieties were not included in the simulation. Furthermore, the hyperfine couplings arising from the two $^{117/119}$Sn nuclei were also not considered in this simulation procedure because the program used did not correct for the above-mentioned second-order effects. As a result, the central line of the triplet, which is hidden under the left branch of the central multiplet, is not taken into account. Nevertheless, the simulated spectrum fits very accurately with the experimental one; see Figure 5. The EPR spectrum thus fully confirmed the proposed composition of the $[Ru(SnPh_3)_2(CO)_2$(iPr-DAB)$]^{\bullet-}$ species, in particular the symmetry equivalence of the two Sn nuclei.

MO Calculations. In order to understand the electronic structure and bonding properties of the parent complex as well as of the radical-anionic product, MO calculations were performed on the model compound $Ru(SnH_3)_2(CO)_2$(H-DAB) and its radical anion. The bond distances and bond angles of this model complex, in which the $SnPh_3$ ligands are replaced by SnH_3, and isopropyl substituents of iPr-DAB by hydrogen atoms, were taken from the crystallographic data of the parent complex, except for the N−H and Sn−H bond distances, for which values of 1.01 and 1.7 Å, respectively, were used.[70] The results of these calculations are presented in Tables 4−6. They were used to construct a qualitative MO scheme shown in Figure 6, which gives a more pictorial insight into the electronic structure and which will be used as a basis for further discussion. Before discussing the characters of the orbitals, it is useful to describe separately the orbitals of the SnH_3 and H-DAB fragments. The relevant orbitals of SnH_3 are the $3a_1$ and 3e orbitals. The $3a_1$ is the singly occupied "sp^3" hybrid; the 3e is a combination of the Sn−H σ bonding orbitals. For the H-DAB ligand, the $2b_1$ is the lowest unoccupied π^* orbital and the $1a_2$ is the highest occupied π orbital.

The symmetric ($sp^3 + sp^3$) combination of the SnH_3 orbitals mixes with the Ru $4d_{z^2}$ orbital while their antisymmetric ($sp^3 - sp^3$) combination interacts with the $5p_z$ metal orbital. Hence, a delocalized three-center, four-electron Sn−Ru−Sn σ-bond is formed. MO calculations show that the HOMO of the complex is the Ru(p_z) + Sn(sp^3−sp^3) combination ($10b_1$) which mixes also with the lowest π^* orbital of H-DAB($2b_1$). The $11b_1$ LUMO orbital is dominated (61%) by the contribution from the $2b_1$ H-DAB π^* orbital with a characteristic admixture of the metal d_{yz} orbital (11%). However, even the LUMO contains a large contribution from the Sn (sp^3−Sp^3) combination (27%) that again results from the $\sigma-\pi^*$ mixing. The $\sigma-\pi^*$ interaction actually gives rise to a strong delocalization of the electron density from the Sn−Ru−Sn σ-bond to the H-DAB ligand that occurs together with of the usual π-back-bonding via the $d_{yz}-\pi^*$ mixing in the occupied $9b_1$ and empty $11b_1$ (LUMO) orbitals.

Calculations on the $[Ru(SnH_3)_2(CO)_2$(H-DAB)$]^{\bullet-}$ radical anion confirmed that the extra electron enters the $11b_1$ LUMO, as expected (Tables 4 and 5). The large positive shift of all the calculated orbital energies is due to the uncompensated effect of the mononegative charge of the radical anion in the vacuum that, however, does not affect the energy differences between the molecular orbitals. These may be readily compared by perusal of the MO-diagrams shown in Figure 7 where the $10b_1$ HOMO of the parent complex and of the radical anion are placed, for clarity, at the same energy. It may be seen that there are only small differences in the relative energies of the orbitals

(68) Nieuwenhuis, H. A. Thesis, University of Amsterdam, 1994.
(69) Goodman, B. A.; Raynor, J. B. *Adv. Inorg. Chem, Radiochem.* **1970**, *13*, 135.
(70) Huheey, J. E. *Inorganic Chemistry, Principles of Structure and Reactivity*, 3rd ed.; Harper and Row: New York, 1983.

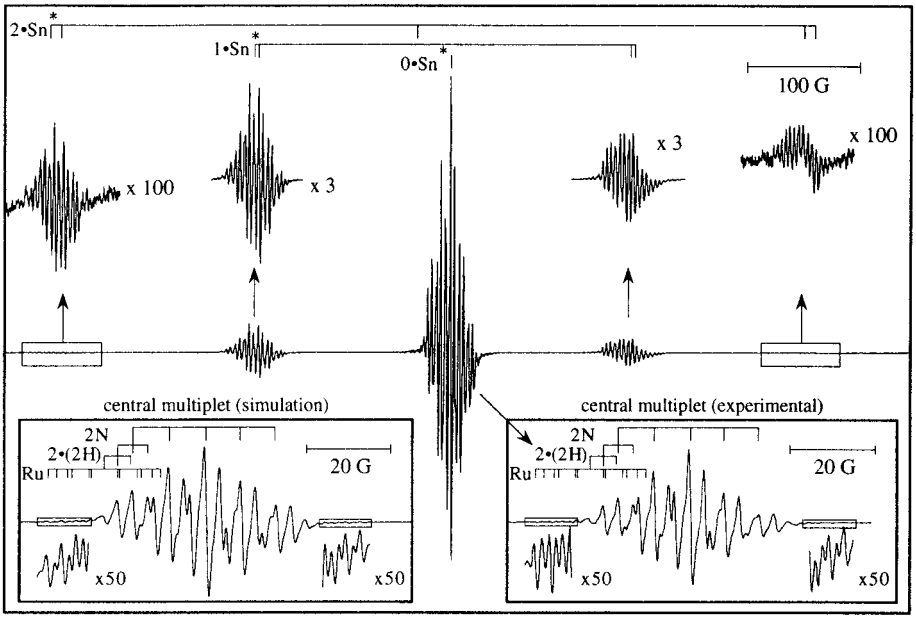

Figure 5. EPR spectrum of $[Ru(SnPh_3)_2(CO)_2(iPr\text{-}DAB)]^{\bullet-}$ in THF at room temperature generated by *in situ* reduction of the parent complex with 1% Na amalgam. Sn* = $^{117/119}$Sn isotopes (modulation amplitude 0.4 G; attenuation 10 dB).

Table 3. EPR Parameters of $[Ru(SnPh_3)_2(CO)_2(iPr\text{-}DAB)]^{\bullet-}$ obtained in THF solution ($g = 1.9960 \pm 0.0002$)

		natural		splitting const (G)		deviation	
nucleus	no.	abundance (%)	spin	exptl	calcd[c]	absolute	%
^{99}Ru	1	12.7	$^5/_2$	5.7[a]	4.14	−1.56	27
^{101}Ru	1	17.1	$^5/_2$	6.4[a]	4.65	−1.75	27
^{117}Sn	2	7.6	$^1/_2$	317.0[b]	344	+27	8
^{119}Sn	2	8.6	$^1/_2$	332.0[b]	360	+28	8
^{14}N	2	99.6	$^1/_1$	8.20[a]	11.59	+3.39	29
^{1}H[e]	2	99.9	$^1/_2$	3.55[a,g]	4.32	+0.77	18
^{1}H[f]	2	99.9	$^1/_2$	3.25[a/g]	*d*	*d*	*d*

[a] Based on the simulated values. [b] Determined from the spectra using the correction factors taken from ref 69. [c] Calculated from the theoretical spin density distribution in $(Ru(SnH_3)_2(CO)_2$(H-DAB) obtained from the DFT calculations. [d] No iPr-*H* in the model compound. [e] Imine proton (C*H*═N(iPr)). [f] iPr proton (C*H*$(CH_3)_2$). [g] We assume that also in the case a_H(CH═N(iPr) > a_H($CH(CH_3)_2$), in agreement with the data collected in Table 8.

below the HOMO but that the energy differences between the HOMO and higher orbitals are clearly different (Tables 4 and 5 and Figure 7). Thus, the calculated energy difference between the HOMO and SOMO of the reduced complex (2.090 eV) is larger than that between the HOMO and LUMO of the parent complex (1.940 eV). The energy difference between the SOMO of the radical anion and its higher-lying orbitals is smaller, compared with that between the LUMO and the higher unoccupied orbitals of the parent complex. Data in Tables 4 and 5 also show that the characters of the $10b_1$ HOMO and $11b_1$ LUMO of the parent complex change only little upon reduction, while the unoccupied $20a_1$ and $19a_1$ orbitals undergo significant redistribution. Notably, a 7% contribution of the H-DAB nitrogen σ-lone-electron pairs ($6a_1$) in the radical-anion suggest even some axial−equatorial σ-delocalization. To understand the charge redistribution in the $Ru(SnH_3)_2(CO)_2$(H-DAB) molecule upon its one-electron reduction, the differences in the valence-electron densities between $Ru(SnH_3)_2(CO)_2$(H-DAB) and $[Ru(SnH_3)_2(CO)_2$(H-DAB)$]^{\bullet-}$ were calculated. The results, summarized in Table 6, clearly show that the electron density at Ru hardly changes. The extra electron density in the radical anion is mainly accepted by the SnH_3 $3a_1$ and H-DAB $2b_1$ orbitals, while a smaller part is spread over the CO ligands via the normal π-back-donation mechanism.

The results of the density functional calculations on the $[Ru(SnH_3)_2(CO)_2$(H-DAB)$]^{\bullet-}$ model compound have been also used to calculate the hyperfine tensor and the isotropic hyperfine splitting constants, using the second order perturbation theory.[61] The splitting constants are shown in Table 3. Even though the calculation somewhat underestimates the values of a_{Ru} and overestimates the a_H and a_N values, the generally good correspondence with the experiment indicates that the conclusions from the MO calculations on the model compound are well applicable to the complex actually studied.

Electronic Absorption Spectra and Their Assignment. The parent complex shows a narrow strong absorption band at 511 nm ($\epsilon = 6000$ M^{-1} cm^{-1}) in THF, shown in Figure 4, which will mainly belong to the HOMO→LUMO transition. This assignment is fully supported by the results of the MO calculations of the transition probabilities which show that the HOMO→LUMO transition is 6.96 and 9.79 times more probable than the energetically close $6a_2$ (d_{xz})→LUMO and $9b_1$ (d_{yz})→LUMO MLCT transitions respectively. (The probabilities of the electronic transitions were obtained by calculating the transition dipole matrix element. The transition probability is directly proportional to the square of this matrix element.) As follows from the characters of HOMO and LUMO (Table 4), the $10b_1$→$11b_1$ transition may be described qualitatively as σ-(Sn−Ru−Sn)→π*. The delocalized nature of the orbitals involved is responsible for a rather small charge-separation in the excited state, which is manifested by a relatively small solvatochromism (710 cm^{-1}; $\lambda_{max} = 508$ nm in CH_3CN and 527 nm in hexane). For comparison, the typical MLCT absorption band of $Ru(Cl)(SnPh_3)(CO)_2$(iPr-DAB) exhibits solvatochromism ca. 2.5 times larger, *i.e.* 1710 cm^{-1}.[62] It should be noted, however, that the shielding effect of the two bulky $SnPh_3$ groups may also diminish the solvatochromism.

Figure 4 reveals that, upon reduction of $Ru(SnPh_3)_2(CO)_2$-(iPr-DAB), the strong band at 511 nm is replaced by two bands of the radical anion at 454 ($\epsilon = 3300$ M^{-1} cm^{-1}) and 652 nm ($\epsilon = 1900$ M^{-1} cm^{-1}), respectively. On the basis of the similarly narrow band shape, the former, high-energy band is assigned to the $10b_1$→$11b_1$ HOMO→SOMO transition that is the counterpart of the HOMO→LUMO transition of the parent species. The low-energy band will then belong to the excitation

Table 4. Characters (%)[a] and Energies of the Relevant MO's of $Ru(SnH_3)_2(CO)_2$(H-DAB)[b]

orbital	description	ϵ (eV)	Ru	SnH_3	H-DAB	CO
$20a_1$	σ* Ru−Sn	−1.400	19% d_{z^2}	46% $3a_1$		23% 2π, 5% 5σ
$19a_1$	σ* Ru−Sn	−1.802	10% $d_{x^2-y^2}$	20% $3a_1$		41% 2π
$13b_2$	2π CO	−2.075	12% p_x, 9% d_{xy}		9% $4b_2$	62% 2π
$11b_1$	π*	**−3.984**	**11% d_{yz}**	**27% $3a_1$**	**61% $2b_1$**	
$10b_1$	**σ Ru−Sn**	**−5.924**	**15% p_z**	**42% $3a_1$**	**27% $2b_1$**	**9% 2π**
$6a_2$	dt_{2g}	−6.509	63% d_{xz}	12% 3e	13% $1a_2$	11% 2π
$9b_1$	dt_{2g}	−7.009	53% d_{yz}	27% 3e	6% $2b_1$	7% 2π
$18a_1$	dt_{2g}	−7.407	67% $d_{x^2-y^2}$			9% 1π, 17% 2π
$12b_2$, $5a_2$, $17a_1$, $8b_1$	Sn−H (4×)	≈−7.7	≈5%	≈85%	≈4%	
$16a_1$	σ Ru−Sn	−7.820	11% 5s, 53% d_{z^2}	7% $2a_1$, 34% $3a_1$		
$4a_2$	π	−9.061	16% d_{xz}	5% 3e	73% $1a_2$	

[a] Based on Mulliken population analyses per MO. [b] The HOMO ($10b_1$) and LUMO ($11b_1$) orbitals are printed in boldface type.

Table 5. Characters (%)[a] and Energies of the Relevant MO's of $[Ru(SnH_3)_2(CO)_2$(H-DAB)$]^{\bullet-}$ [b]

orbital	description	ϵ (eV)	Ru	SnH_3	H-DAB	CO
$20a_1$	σ* Ru−Sn	2.224	6% d_{z^2}, 42% 6s	18% $3a_1$	7% $6a_1$[c]	17% 2π
$19a_1$	σ* Ru−Sn	2.107	11% d_{z^2}, 7% $d_{x^2-y^2}$	32% $3a_1$	7% $6a_1$[c]	27% 2π
$13b_2$	2π CO	1.896	10% p_x, 6% d_{xy}		7% $4b_2$	68% 2π
$11b_1$	***π****	**0.300**	**9% d_{yz}**	**25% $3a_1$**	**66% $2b_1$**	
$10b_1$	**σ Ru−Sn**	**−1.790**	**12% p_z**	**49% $3a_1$**	**24% $2b_1$**	
$6a_2$	dt_{2g}	−2.319	62% d_{xz}	5 % 3e	19% $1a_2$	11% 2π
$9b_1$	dt_{2g}	−2.887	60% d_{yz}	11% 3e	4% $2b_1$	12% 2π
$18a_1$	dt_{2g}	−3.284	68% $d_{x^2-y^2}$			7% 1π, 20% 2π
$17a_1$	σ Ru−Sn	−3.656	10% 5s, 43% d_{z^2}	4% $2a_2$, 40% $3a_1$		
$12b_2$, $5a_2$, $8b_1$, $16a_1$	Sn−H (4×)	≈−3.9	≈5%	≈85%	≈4%	
$4a_2$	π	−4.714	19% d_{xz}	19% 3e	56% $1a_2$	

[a] Based on Mulliken population analyses per MO. [b] The HOMO ($10b_1$) and SOMO ($11b_1$) orbitals are printed in boldface type. [c] Symmetric combination of nitrogen lone electron pairs.

Table 6. Changes in Valence-Electron Density (Δq) of $Ru(SnH_3)_2(CO)_2$(H-DAB) upon One-Electron Reduction[a]

orbitals	Ru 5s	Ru $4p_y$	Ru $4p_x$	Ru $4p_z$	Ru $4d_{z^2}$	Ru $4d_{x^2-y^2}$	Ru $4d_{xy}$	Ru $4d_{yz}$	Ru $4d_{xz}$
Δq[b]	−0.04	−0.02	−0.01	−0.05	−0.05	−0.05	+0.01	+0.07	−0.05

orbitals	SnH_3 $3a_1$	SnH_3 e	DAB a_1	DAB a_2	DAB $2b_1$	DAB b_2	CO σ	CO π
Δq[b]	**+0.59**	+0.07	−0.05	−0.02	**+0.51**	−0.04		**+0.12**

[a] Based on Mulliken population analysis. [b] Change in valence-electron density upon reduction.

of the unpaired electron from the SOMO to the higher empty orbitals, most probably the σ*(Sn−Ru−Sn) $19a_1$ and/or $20a_1$. (Note that the transition to the $13b_2$ orbital is symmetry forbidden.) This assignment is qualitatively supported by the MO calculations which show that the energy difference between the HOMO and SOMO in the radical anion of the model compound is larger by 0.283 eV (2280 cm^{-1}) than the difference between the $19a_1$ orbital and the SOMO ($11b_1$). Also, the energy difference between the HOMO and SOMO in the radical anion is larger by 0.15 eV (1210 cm^{-1}) than between the HOMO and LUMO of the parent complex, in qualitative agreement with the high-energy shift of the $10b_1 \rightarrow 11b_1$ transition by some 2460 cm^{-1} observed experimentally; see Figure 4.

Discussion

In the preceding chapters, the synthesis, structure, spectroscopic, and (spectro-) electrochemical properties of an unprecedented inorganometallic complex containing a nearly linear Sn−Ru−Sn unit oriented perpendicular to the Ru(DAB) chelate ring have been described. The MO calculations on the $Ru(SnH_3)_2(CO)_2$(H-DAB) model compound and its radical anion revealed the most important aspects of the electronic structure of these two complexes, namely the strong electron donation from the $SnPh_3$ ligands and the extensive mixing of the σ(Sn−Ru−Sn) and DAB π* orbitals in both the HOMO and LUMO (SOMO). These unique electronic features, which are absent in carbonyl−diimine complexes that lack strongly σ-bonded axial ligands, appear to be responsible for most of the unusual properties of $Ru(SnPh_3)_2(CO)_2$(iPr-DAB) and its radical anion.

Thus, the donation of electron density from the Sn−Ru−Sn unit to the π*-DAB orbital manifests itself already in the molecular structure of $Ru(SnPh_3)_2(CO)_2$(iPr-DAB) which shows longer C═N and shorter C(1)−C(2) bonds of the iPr-DAB ligands than analogous complexes not containing *trans*-σ-bonded ligands, like Ru(Cl)$(SnPh_3)(CO)_2$(iPr-DAB) and Ru(I)(Me)-$(CO)_2$(iPr-DAB).[62,71] These differences in bond-lengths are in accordance with the C═N antibonding and C(1)−C(2) bonding character of the DAB-$2b_1$ π* orbital.

Also, the ν(CO) wavenumbers of $Ru(SnPh_3)_2(CO)_2$(iPr-DAB) are relatively low, reflecting a larger electron density on the Ru atom. The $\sigma-\pi$* interaction also changes the character of the electronic transition responsible for the visible absorption band. For most of the carbonyl-diimine complexes studied previously, such a band belongs to MLCT transitions. In Ru-$(SnPh_3)_2(CO)_2$(iPr-DAB) and also $[Ru(SnPh_3)_2(CO)_2$(iPr-DAB)$]^{\bullet-}$, the HOMO→LUMO (SOMO) transition occurs between the delocalized $10b_1$ and $11b_1$ orbitals that both contain significant $SnPh_3$ contribution. This change in character of the electronic transition is manifested by a higher extinction coefficient and smaller solvatochromism of the absorption band, as compared, *e.g.*, with Ru(Cl)$(SnPh_3)(CO)_2$(iPr-DAB).[62]

The up-field shift of the imine-proton in the ^{1}H NMR spectrum, and the increased value of the $^4J(^{117/119}Sn,H)$ coupling

(71) Kleverlaan, C. J.; et al. Unpublished results.

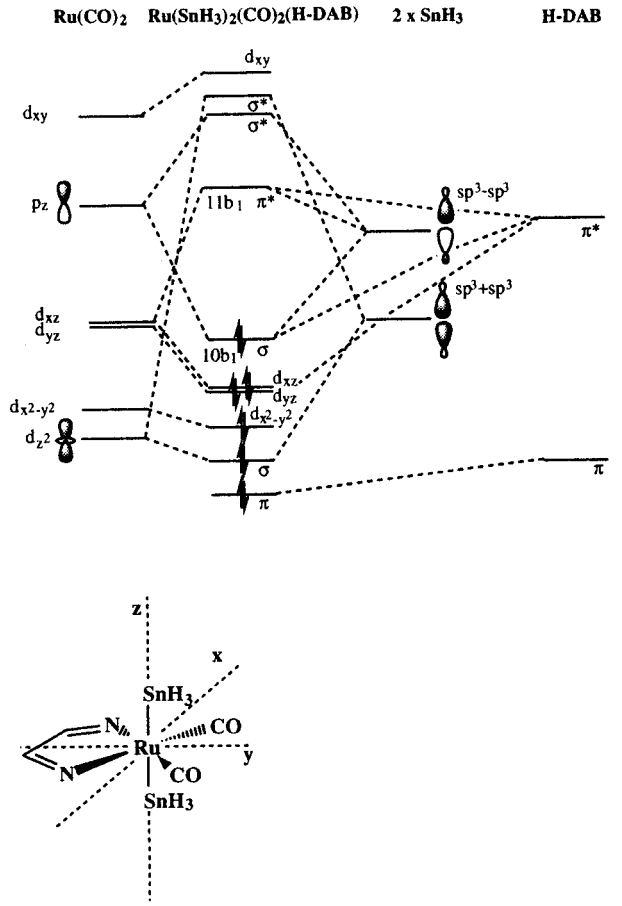

Figure 6. Qualitative MO scheme of $Ru(SnH_3)_2(CO)_2$(H-DAB) and chosen orientation of the axes.

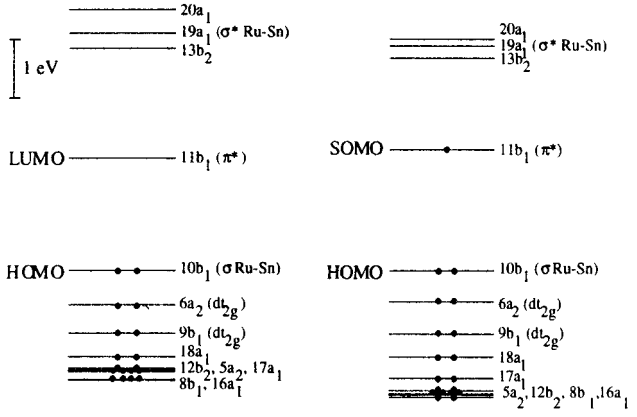

Figure 7. MO diagrams of $Ru(SnH_3)_2(CO)_2$(H-DAB) and $[Ru(SnH_3)_2(CO)_2$(H-DAB)$]^{\bullet-}$, based on DFT calculations. The HOMO's are positioned at the same energy level.

constants also reflect this delocalized character of the Ru−DAB chelate ring.[72]

The value of the reduction potential ($E_{1/2} = -1.86$ V *vs* Fc/Fc^+ in THF), which is more negative than those found for most of known DAB-complexes,[3,12,68,73,74] is also in line with the strong $\sigma-\pi^*$ interaction which changes the character of LUMO and increases its energy because of a mixing between the σ-(Sn−Ru−Sn) and π^*-DAB orbitals. For comparison, Ru(I)(Me)-$(CO)_2$(iPr-DAB) is reduced considerably more positively ($E_{1/2} = -1.55$ V *vs* Fc/Fc^+ in THF)[12,68,74] in accordance with its lower LUMO energy relative to $Ru(SnPh_3)_2(CO)_2$(iPr-DAB). This comparison reflects the difference between the bonding properties of the two complexes where the LUMO of Ru(I)(Me)-$(CO)_2$(iPr-DAB) has a major contribution from the lowest π^* orbital of iPr-DAB whereas the LUMO of the $Ru(SnPh_3)_2(CO)_2$-(iPr-DAB) possesses a significantly mixed iPr-DAB/$SnPh_3$ character. The Ru(Cl)$(SnPh_3)(CO)_2$(iPr-DAB) complex is also reduced much more positively ($E_{1/2} = -1.48$ V *vs* Fc/Fc^+ in THF)[36] than $Ru(SnPh_3)_2(CO)_2$(iPr-DAB). This comparison clearly shows that it is the simultaneous presence of two axial covalent Ru−Sn bonds that leads to the $\sigma-\pi^*$ interaction and, hence, to a rise in the LUMO energy and drop in the reduction potential. Interestingly, rather negative reduction potentials were also found for other DAB complexes that contain σ-bonded ligands like Re(Me)$(CO)_3$(iPr-DAB) ($E_{1/2} = -1.74$ V *vs* Fc/Fc^+ in nPrCN)[73] and $Pt(Me)_4$(c-hexyl-DAB) ($E_{1/2} = -1.93$ V *vs* Fc/Fc^+ in CH_3CN).[21]

One of the most spectacular features of $Ru(SnPh_3)_2(CO)_2$-(iPr-DAB) is its reduction to intrinsically stable $[Ru(SnPh_3)_2$-$(CO)_2$(iPr-DAB)$]^{\bullet-}$. Analogous Ru(L)(L′)$(CO)_2$(α-diimine)[12,68] complexes undergo facile ligand dissociation upon reduction, whereas σ-bonded Re and Pt species (*e.g.* Re$(SnPh_3)(CO)_3$(1,-10-phenanthroline),[75] $Pt(Me)_4$(c-hexyl-DAB)[21]) are also reversibly reduced to rather stable radical anions. The results of the MO calculations clearly show that the remarkable stability of $[Ru(SnPh_3)_2(CO)_2$(iPr-DAB)$]^{\bullet-}$ originates in the large capacity of the $SnPh_3$ and DAB ligands and, to a lesser extent, of the CO ligands to accommodate the extra electron density conferred upon the $Ru(SnPh_3)_2(CO)_2$(iPr-DAB) molecule by its one-electron reduction. This effect is well documented by the calculated differences of the Mulliken valence-electron densities in inidividual orbitals between the $Ru(SnH_3)_2(CO)_2$(H-DAB) model compound and its radical anion (Table 6). It is also evidenced by the negative shift of ν(CO) wavenumbers (by about 34 cm^{-1}) upon reduction, that is caused by the increased Ru→CO π-back-bonding and, most of all, by the hyperfine splitting constants determined from the EPR spectrum of $[Ru(SnPh_3)_2(CO)_2$(iPr-DAB)$]^{\bullet-}$. These splitting constants reflect the localization of the spin density on individual atoms in the molecule, *i.e.* the localization of the SOMO wavefunction. Assuming that the SOMO of $[Ru(SnPh_3)_2(CO)_2$(iPr-DAB)$]^{\bullet-}$ and the LUMO of $Ru(SnPh_3)_2(CO)_2$(iPr-DAB) have similar

Table 7. EPR Parameters of Selected Radical Compounds Containing Ru or Sn Hyperfine Splitting Constants

compound	$a_{(^{99/101}Ru)}$ (G)	*g*	conditions	ref
$[RuCp(CO)_2N(O)R]^{\bullet}$	5.04/5.70	2.0078	toluene, room temp	80
$[Ru(SiMe_3)(CO)_4N(O)R]^{\bullet}$	≈5	2.0048	toluene, 313 K	81
$[Ru(bpy)(CN)_4]^{3-}$	3.0	1.999	DMF, room temp	82
$[Ru(bpz)(CN)_4]^{3-}$	4.58/5.14	1.9934	MeCN, room temp	76
$[Ru(PPh_3)_2(CO)_2(o\text{-}O_2C_6Cl_4)]^{\bullet+}$	3.7	2.002	CH_2Cl_2, room temp	83

compound	$a_{(^{117}Sn)}$ (G)	$a_{(^{119}Sn)}$ (G)	*g*	conditions	ref
$Sn^{\bullet}(N(SiMe_3)_2)_3$	3176	3426	2.0094	C_6H_6, 293 K	84
$Sn^{\bullet}(CH(SiMe_3)_2)_3$	1698	1776	1.9912	C_6H_6, 293 K	84
$(Me_3)SnCH_2C^{\bullet}H_2$	467.7	488.9	2.00205	172 K	85
$(Me_3)SnC^{\bullet}H_2$	132.5	137.0	*a*	203 K	86

[a] Not reported.

(72) tom Dieck, H.; Renk, I. W.; Franz, K. D. *J. Organomet. Chem.* **1975**, *94*, 417.
(73) Rossenaar, B. D.; Hartl, F.; Stufkens, D. J. *Organometallics*, submitted for publication.
(74) tom Dieck, H.; Rohde, W.; Behrens, U. *Z. Naturforsch.* **1989**, *44B*, 158.
(75) Luong, J. C.; Faltynek, R. A.; Wrighton, M. S. *J. Am. Chem. Soc.* **1979**, *101*, 1597.

Table 8. EPR Parameters of Some Largely R-DAB Localized Radicals Related to $[Ru(SnPh_3)_2(CO)_2(iPr\text{-}DAB)]^{\bullet-}$

compound	Hyperfine splitting constants (G) a_M	a_N	a_H[a]	a_H[b]	a_x[c]	g	conditions	ref
$[iPr\text{-}DAB]^{\bullet-}$		5.47	4.79	3.74		2.0034	Et_2O, 293 K	87
$[tBu\text{-}DAB]^{\bullet-}$		5.6	4.3	0.15		2.0035	THF	88
$[Zn(Et)(tBu\text{-}DAB)]^{\bullet}$		4.87	5.87		0.48, a_H[d]	*e*	$T > 223$ K	89,90
$[Zn(Cl)(tBu\text{-}DAB)]^{\bullet}$ [f]	4.4	5.60	5.6		0.58, a_{Cl}	2.0024	THF, 213−303 K	88
$[Mo(CO)_4(iPr\text{-}DAB)]^{\bullet-}$		6.84	4.1	1.52		2.0039	THF, 298 K	3
$[Mo(CO)_3(PBu_3)(tBu\text{-}DAB)]^{\bullet-}$	2.95	6.96	3.95		44.1, *ap*	*g*	DMF, 293 K	77
$[Mo(CO)_3(PBu_3)_2(tBu\text{-}DAB)]^{\bullet-}$	3.1	6.8	4.0		45.0, *ap*	*g*	DMF, 293 K	77
$[Re(CO)_3(tBu\text{-}DAB)]^{\bullet}$	35.55	7.34	5.03			2.0046	cyclohexane, 343 K	91
$[Cr(CO)_4(iPr\text{-}DAB)]^{\bullet-}$		7.4	4.0	1.65		2.0031	DME, 253 K	3
$[Mn(CO)_3(tBu\text{-}DAB)]^{\bullet}$	8.47	7.48	4.35			2.0043	toluene, 203 K	91
$[Pt(Me)_4(cHexcyl\text{-}DAB)]^{\bullet-}$	61.2	8.20	4.20			1.9945	THF, 295 K	21
$[Ru(SnPh_3)_2(CO)_2(iPr\text{-}DAB)]^{\bullet-}$	6.40	8.20	3.55	3.25	≈325, a_{Sn}	1.9960	THF, 293 K	this work

[a] The hyperfine splitting of the C*H*═NR proton of the R-DAB ligand. [b] Additional hyperfine splitting of the C(CH_3)$_3$ protons in tBu-DAB complexes, and the C*H*(CH_3)$_2$ protons in iPr-DAB complexes. [c] Additional splitting. [d] αH of the ethyl group. [e] Not reported. [f] ^{67}Zn enriched. [g] *g* value between 2.000 and 2.010.

characters, as is substantiated by the MO calculations (Tables 4 and 5), the EPR spectrum also affords indirect information on the LUMO of the $Ru(SnPh_3)_2(CO)_2(iPr\text{-}DAB)$ parent. To put the measured hyperfine splitting constants (Table 3) in a broader perspective, a comparison is made with previously reported hyperfine splitting constants of some radical species containing Sn or Ru atoms and/or α-diimine ligands (see Tables 7 and 8).

The value of the Ru hyperfine splitting constant, $a_{Ru} = 6.4$ G, measured for $[Ru(SnPh_3)_2(CO)_2(iPr\text{-}DAB)]^{\bullet-}$ is only slightly larger than the a_{Ru} values of Ru^{II} complexes with coordinated ligand-localized radicals collected in Table 7. This is in accordance with the proposed dominant localization of the $11b_1$ SOMO on the iPr-DAB and $SnPh_3$ ligands together with the positive contribution from the $\sigma-\pi^*$ mixing that would not occur in complexes lacking σ-bonded ligands.

Comparing the $^{117/119}$Sn hyperfine splitting of $[Ru(SnPh_3)_2(CO)_2(iPr\text{-}DAB)]^{\bullet-}$ (317 and 332 G, respectively) with some data taken from the literature (Table 7), we see that the radicals, in which the unpaired electron is dominantly localized on the Sn atom, exhibit only 5−10 times larger Sn hyperfine splitting constant. The splitting constant a_{Sn} rapidly decreases when the unpaired electron is more localized on the α-carbon atom as in $Me_3SnC^{\bullet}H_2$, and increases again when localized on the β-carbon atom (Table 7). The still rather large a_{Sn} is a very remarkable feature of the EPR spectrum of $[Ru(SnPh_3)_2(CO)_2(iPr\text{-}DAB)]^{\bullet-}$. It may be readily explained by the $\sigma\pi^*$ delocalization, *i.e.* the large (25 %) participation of the Sn sp^3 orbital in the SOMO predicted by the MO calculations. Further information on the relative magnitude of this effect, in relation to other radical complexes, can be obtained from the a/A_{iso} ratios.[76] The ratio of 0.044 obtained for both $a_{(^{117}Sn)}/A_{iso(^{117}Sn)}$ and $a_{(^{119}Sn)}/A_{iso(^{119}Sn)}$ in $[Ru(SnPh_3)_2(CO)_2(iPr\text{-}DAB)]^{\bullet-}$, is considerably larger than the ratio of $a_{(^{31}P)}/A_{iso(^{31}P)}$ (0.012) in $[Mo(PBu_3)_2(CO)_2(tBu\text{-}DAB)]^{\bullet-}$[77] ($A_{iso(^{117}Sn)} = -7268$, $A_{iso(^{119}Sn)} = -7603$, $A_{iso(^{31}P)} = 3676$);[69] see Table 8. The much larger spin density on Sn in the former complex compared to that on P in the latter one may be related to the higher energy of the a_1 (sp^3) σ-donor orbital of $SnPh_3$ in comparison with that of PBu_3, giving rise to a stronger $\sigma-\pi^*$ mixing in $[Ru(SnPh_3)_2(CO)_2(iPr\text{-}DAB)]^{\bullet-}$ than in $[Mo(PBu_3)_2(CO)_2(tBu\text{-}DAB)]^{\bullet-}$. These observations fully support the above conclusions on the high capacity of the $SnPh_3$ ligands to accommodate the extra electron density in the radical anion.

The coupling constants collected in Table 8 provide information about the SOMO distribution over the M-(DAB) chelate ring of the radical anion. In view of the fact that a_N and a_H constants of $iPr\text{-}DAB^{\bullet-}$ and $tBu\text{-}DAB^{\bullet-}$ closely resemble one another, a comparison is made with related tBu-DAB complexes. It is obvious from Table 8 that large values of a_N are accompanied by small values of a_H and *vice versa*. This reflects the variable spin density in the π^* SOMO on the carbon or the nitrogen atoms. The large a_N and small a_H values for $[Ru(SnPh_3)_2(CO)_2(iPr\text{-}DAB)]^{\bullet-}$ demonstrate that a large part of the spin density on the DAB skeleton is localized on the nitrogen atoms, reflecting thus the $\sigma\rightarrow\pi^*$ donation of the spin density.

In contrast to the *g* values of most of the DAB complexes listed in Table 8, the *g* value of 1.9960 found for $[Ru(SnPh_3)_2(CO)_2(iPr\text{-}DAB)]^{\bullet-}$ is considerably smaller than the free electron value, $g_e = 2.0023$. It lies much closer to the *g* value of $[Pt(Me)_4(cHexyl\text{-}DAB)]^{\bullet-}$.[21] This small value is due to the spin-orbit interaction that arises from the presence of three heavy atoms. The negative sign of the *g* deviation from the g_e value indicates that the spin−orbit coupling dominantly involves the admixture of higher unoccupied orbitals[78,79] with a significant contribution from the Ru and Sn orbitals ($19a_1$, $20a_1$), rather than of lower, doubly occupied ones, into the SOMO. This observation is in full accordance with the results of the MO calculations which show that the HOMO−SOMO energy gap is larger than the separation between the SOMO and the next two unoccupied orbitals by 0.49 and 0.28 eV respectively. The visible absorption spectrum of $[Ru(SnPh_3)_2(CO)_2(iPr\text{-}DAB)]^{\bullet-}$ points to the same conclusion, showing the HOMO→SOMO transitions at a significantly higher energy than the SOMO→$19a_1$/$20a_1$ transition. In a forthcoming article it will be demonstrated

(76) Waldhör, E.; Poppe, J.; Kaim, W.; Cutin, E. H.; Garía Posse, M. E.; Katz, N. E. *Inorg. Chem.* **1995**, *34*, 3093.
(77) tom Dieck, H.; Franz, K. D.; Hohmann, F. *Chem. Ber.* **1975**, *108*, 163.
(78) Kaim, W. *Coord. Chem. Rev.* **1987**, *76*, 187.
(79) Kaim, W.; Kohlmann, S. *Inorg. Chem.* **1990**, *29*, 2909.
(80) Sostero, S.; Rehorek, D.; Polo, E.; Traverso, O. *Inorg. Chim. Acta* **1993**, *209*, 171.
(81) Hudson, A.; Lappert, M. F.; Lednor, P. W.; MacQuitty, J. J.; Nicholson, B. K. *J. Chem. Soc., Dalton Trans.* **1981**, 2159.
(82) Samuels, A. C.; DeArmond, M. K. *Inorg. Chem.* **1995**, *34*, 5548.
(83) Connelly, N. G.; Manners, I.; Protheroe, J. R. C.; Whiteley, M. W. *J. Chem. Soc., Dalton Trans.* **1984**, 2713.
(84) Cotton, J. D.; Cundy, C. S.; Harris, D. H.; Hudson, A.; Lappert, M. F. *J. Chem. Soc., Chem. Commun.* **1974**, 651.
(85) Kawamura, T.; Kochi, J. K. *J. Am. Chem. Soc.* **1972**, *94*, 648.
(86) Hudson, A.; Hussain, H. A. *J. Chem. Soc.* **1969**, *B*, 793.
(87) de Klerk-Engels, B.; Hartl, F.; Vrieze, K. *Inorg. Chim. Acta*, in press.
(88) Clopath, P.; von Zelewsky, A. *Helv. Chim. Acta* **1972**, *55*, 52.
(89) Jastrzebski, J. T. B. H.; Klerks, J. M.; van Koten, G.; Vrieze, K. *J. Organomet. Chem.* **1981**, *210*, C49.
(90) Klerks, J. M.; Jastrzebski, J. T. B. H.; van Koten, G.; Vrieze, K. *J. Organomet. Chem.* **1982**, *224*, 107.
(91) Andréa, R. R.; de Lange, W. G. J.; van der Graaf, T.; Rijkhoff, M.; Stufkens, D. J.; Oskam, A. *Organometallics* **1988**, *7*, 1100.

that this delocalized character of HOMO and LUMO has also a dramatic effect on the excited state properties of the neutral parent complex.

Conclusions

The simultaneous presence of two *trans*-oriented Ru−Sn σ-bonds influences profoundly the bonding within the $Ru(SnPh_3)_2(CO)_2$(iPr-DAB) molecule and leads to an electronic structure that is unprecedented among substituted metal carbonyl diimine complexes known. Its main features are a delocalized 3-center, 4-electron Sn−Ru−Sn σ-bond and an extensive mixing of the Ru−d(π), Ru−$5p_z$, Sn−sp^3, and DAB−π^* characters in both the HOMO and LUMO, which results in a delocalization of the σ-electron density on the iPr-DAB ligand. Reduction of $Ru(SnPh_3)_2(CO)_2$(iPr-DAB) affords a radical anion that has approximately the same molecular and electronic structure as the parent molecule. The remarkable stability of the radical anion stems from the strength of the Sn−Ru−Sn bond and from the highly delocalized character of the SOMO (*i.e*. LUMO of the parent complex) which allows the accommodation of the extra electron density on the $SnPh_3$, iPr-DAB, and, to a lesser extent, CO ligands.

Acknowledgment. The Netherlands Foundation for the Chemical Research (SON) and the Netherlands Organisation for Advancement of Pure Research (NWO), together with COST D4 Action and European Scientific Network Program, are thanked for financial support. We also thank Dr. S. P. J. Albracht of the E. C. Slater Institute for Biochemical Research for his assistance with the EPR measurements.

Supporting Information Available: Listing of the fractional coordinates and thermal parameters for $Ru(SnPh_3)_2(CO)_2$(iPr-DAB) and the hydrogen atom parameters, bond distances, and bond angles (11 pages). Ordering information is given on any current masthead page.

IC960042H